Nokhbeh, S. R., Gholizadeh, M., Salimi, A., & Sparkes, H. A. (2019). Crystal structure, characterization, Hirshfeld surface analysis and DFT studies of two [propane 3-bromo-1-(triphenyl phosphonium)] cations containing bromide (I) and tribromide (II) anions: The anion (II) as a new brominating agent for unsaturated compounds. *Journal of Molecular Structure*, *1195*, 542-554. https://doi.org/10.1016/j.molstruc.2019.05.127

# Crystal structure, characterization, Hirshfeld surface analysis and DFT studies of two [Propane 3-bromo-1-(triphenyl phosphonium)] cations containing bromide (I) and tribromide (II) anions: The anion (II) as a new brominating agent for unsaturated compounds

Seyed Reza Nokhbeh[1], Mostafa Gholizadeh[1*], Alireza Salimi[1], Hazel A. Sparkes[2]

[1]*Department of Chemistry, Faculty of Science, Ferdowsi University of Mashhad, Mashhad I. R, Iran*

[2]*School of Chemistry, University of Bristol, Cantock's Close, Bristol BS8 1TS, UK*

✉ Corresponding Author (Mostafa Gholizadeh): m_gholizadeh@um.ac.ir

## Abstract

In this study, propane 3-bromo-1- (triphenyl phosphonium) bromide, I, and propane 3-bromo-1- (triphenyl phosphonium) tribromide, II, (II as a new brominating agent) were synthesized and characterized by $^{1}$H-NMR, $^{13}$C-NMR, $^{31}$P-NMR, FT-IR spectroscopy, Thermogravimetric Analysis, Differential Thermal Analysis, Differential Scanning Calorimetry and single crystal X-ray analysis. Density Functional Theory calculations (energy, structural optimization and frequencies, Natural Bond Orbital, absorption energy and binding energy) were performed by using B3LYP/ 6-311 ++G (d, p) level of theory. Hirshfeld surface analysis and fingerprint plots were utilized to investigate the role of bromide and tribromide anions on the crystal packing structures of title compounds. The results revealed that the change of accompanying anionic moiety can affect the directional interactions of C-H···Br hydrogen bonds between anionic and cationic units in which the H···Br with a proportion of 53.8% and 40.9% have the major contribution in the stabilization of crystal structures of I and II, respectively. Furthermore, the thermal stability of new

brominating agent II with tribromide anion was compared with compound I with bromide anion. Nontoxicity, short reaction time, thermal stability, simple working up and high yield are some of the advantages of these salts.

Keywords: phosphonium tribromide, crystal structure, brominating agent, Hirshfeld surface analysis, DFT calculations

## 1. Introduction

In recent decades quaternary phosphonium [1], ammonium [2, 3], pyridinium [4] and immidazolium [5] salts are widely used as phase transfer catalysts [6-9] and reagents in the synthesis of organic compounds [5]. Phosphonium salts, especially their ionic liquids [5, 10], play an important role in organic synthesis [11-14], different fields of industries [15-18] and medicine [1, 8, 19]. These salts show a range of interesting properties including ease of synthesis, very good thermal stability, favourable environmental aspects, miscibility with water and polar organic solvents, electrochemical stability [20], high viscosity and low vapor pressure. Because of their distinctive properties, these organic salts are attracting increasing attention in many fields particularly in organic chemistry. Unlike inorganic reagents that are generally insoluble in most organic solvents, this type of organic salts are completely soluble in common polar organic solvents and therefore can be used successfully as surfactants for organic transformations.

Quaternary ammonium and phosphonium salts ($R_4N^+X^-$ or $R_4P^+X^-$) are especially valuable because they are somewhat soluble in both water and polar organic solvents. They are used as phase transfer catalysts to move ionic nucleophiles and bases in to organic media. A phase transfer catalyst facilitates reaction in which one of the reactants is insoluble in aqueous solutions and another is insoluble in organic solutions. The cation of phase transfer salt forms an ion pair with an anion, and the large alkyl or aryl groups in ammonium or phosphonium ion lend solubility in organic phase. In the organic phase anion is more reactive than in the aqueous phase because it is stripped of its solvating water molecules. Halogenating,

oxidative or reductive anions can be transferred in to the organic phases by the use of a suitable ammonium or phosphonium cations as phase transfer catalysts. Indeed cation plays as a carrier to transfer anion to organic media. As the length of the alkyl groups increases, the water solubility decreases. Therefor we can tune the solubility of salts with precisely selection of alkyl or aryl groups on the cation.

With a suitable choice from many different cations and related counterions, phosphonium salts can be utilized as oxidative, reductive or halogenating agents with good selectivity, mild reaction conditions and acceptable yields. Although bromination of organic substrates are usually carried out by molecular bromine but the new generation of phosphonium and ammonium tribromides are synthesized and used for this goal [2, 3, 10, 14, 21-27] so we prepared and used a new phosphonium tribromide for bromination of double bonds. Tribromides are more suitable than the liquid bromine because of their crystalline nature, hence it makes it easier to store, transport, and maintain the desired stoichiometry. Instead of bromination with non-selective elemental bromine under harsh condition, organic phosphonium tribromides as well as ammonium and immidazolium tribromides were used to brominate the C-C double bonds and aromatic rings using mild conditions and in a selective manner [10, 26, 27]. The bromination of double bonds by liquid bromine or by tribromide salts has a different mechanisms, thermodynamics and kinetics. Although, bromination of cyclohexene by $Br_2$ and $Br_3^-$ in 1, 2-dichloroethane have large negative entropies ($\Delta S^{\ddagger}$ = -62.0 eu. and $\Delta S^{\ddagger}$ = -40.9 eu. respectively), for bromination with $Br_2$ there is a negative activation parameters and enthalpy ($E_a$ = -7.8 kcal/ mol, $\Delta H^{\ddagger}$ = -8.4 kcal/ mol), while $Br_3^-$ has positive values ($E_a$ = +6.6 kcal/ mol, $\Delta H^{\ddagger}$ = +6.0 kcal/ mol). Thus third -order and second -order rate constants are obtained for the reactions of free bromine and tribromide (respectively) in different solvents. With respect to the kinetic and thermodynamic evidence, belluchi proposed two different mechanisms for bromination with $Br_2$ and by tribromide anion.[28].

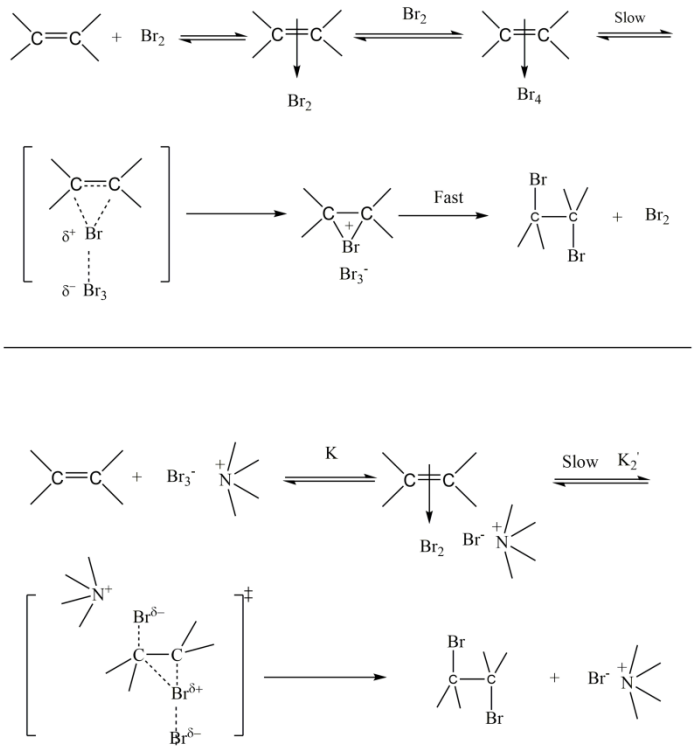

Scheme 1. Two different mechanisms for bromination of double bonds with $Br_2$ and by tribromide anion.

Solid nontoxic phosphonium monocationic and dicationic moieties with tribromide anion including benzyl triphenyl phosphonium tribromide (BTPPT) [21], ethyl triphenyl phosphonium tribromide (ETPPT) [25], methyl triphenyl phosphonium tribromide (MTPPT) [23], tridecyl methyl triphenyl phosphonium tribromide (TMTPPT) [24] and 1, 2-ethylene bis (triphenyl phosphonium) ditribromide (EBTPPDT) [27], have all been used as mild brominating and oxidizing agents for the selective bromination of C-C multiple bonds and aromatic rings, these reactions are more favourable than using the very active, non–selective and toxic molecular bromine under harsh conditions. Reusability of tribromide salts is one of the interesting factors that predominate over molecular bromine as these salts can be used and recycled several times without any significant decrease in their performances.

The structural aspects of these salts were investigated by several experimental and theoretical methods including X-ray crystallography and DFT calculations. Hirshfeld surface analysis was also employed. This type of calculation is a convenient tool for the investigation of intermolecular interactions. Herein, we

report the synthesis, characterization ($^{1}$H NMR, $^{13}$C NMR, $^{31}$P NMR, FT-IR, and TG/DTA/DSC), single crystal X-ray and DFT studies of propane 3-bromo-1-(triphenyl phosphonium) bromide, I, and propane 3-bromo-1-(triphenyl phosphonium) tribromide, II, (II as mild, inexpensive and efficient brominating agent). In addition, Hirshfeld surface and 2D fingerprint plots are presented to highlight short intermolecular contacts in the crystal structures. In addition, the use of a new salt to brominate double bonds is presented with excellent yields.

## 2. Results and discussion

Initially, propane 3-bromo-1-(triphenyl phosphonium) bromide, I, was synthesized as a white powder and recrystallized in hot water (85-88% yield, m.p. 230-232 ºC by DSC) (Fig. 1), and then treated with potassium tribromide in aqueous solution. Yellow precipitate propane 3-bromo-1-(triphenyl phosphonium) tribromide, II, was formed, filtered and air dried overnight. DSC thermogram was taken (Fig. 2) (94-96 % yield, m.p. 149-151 ºC) Scheme 1.

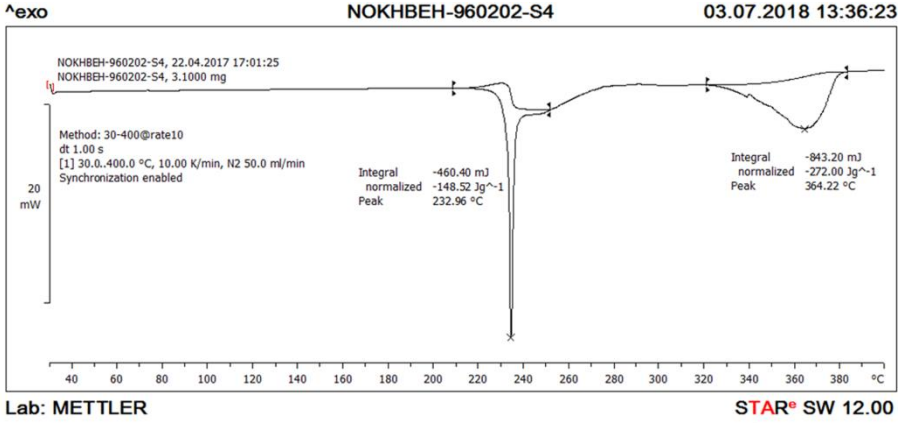


Fig. 1. DSC thermogram of compound I.

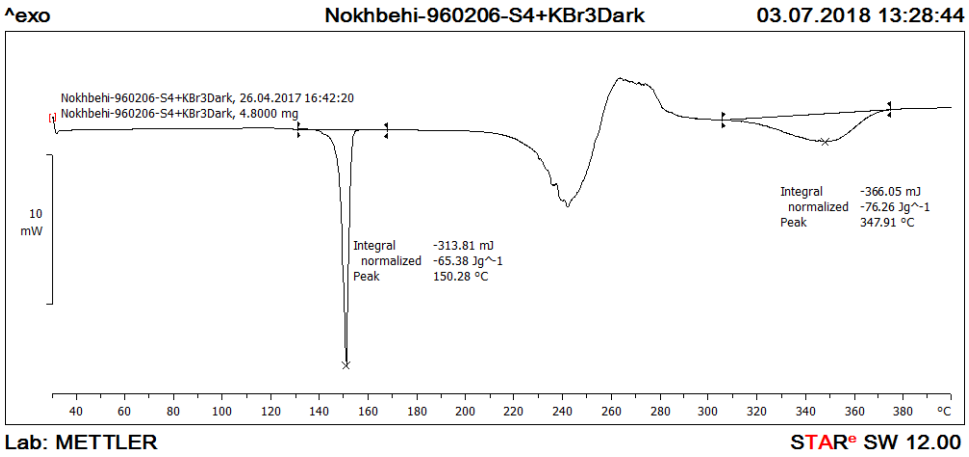


Fig. 2. DSC thermogram of compound II.

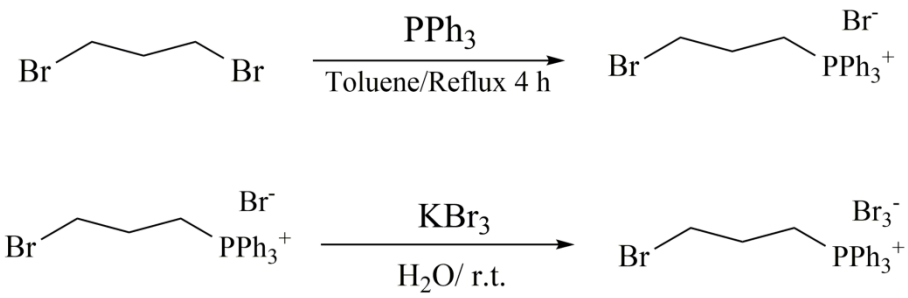


Scheme 2. Schematic reaction for preparation of propane 3-bromo-1-(triphenyl phosphonium) bromide, I, and tribromide, II.

### 2.1. Crystal structure description

The single crystal X-ray analysis of I revealed that this compound crystallizes in the monoclinic crystal system in the $P2_1/c$ space group with Z'=1, Z = 4. The asymmetric unit contains one propane 3-bromo-1-(triphenyl phosphonium) cation and one bromide anion (1:1 ratio of cationic to anionic units). The ORTEP view of compound I is shown in Fig. 3a. The phosphorous atom of the cation exhibit a slightly distorted tetrahedral geometry, with the bond angles around the P atoms in the range from 107.23(7)$^o$ to 111.19(7)$^o$. The geometry of cation (bond lengths and angles) is general and comparable with our previously reported [27]. The 3D supramolecular network of this compound is dominated by the variety of C-H···Br hydrogen bonds. In addition, C-H···π interactions, which can play a crucial role in the stabilization of supramolecular

assemblies, are found to be present (Fig. 3b). The bromide anions each formed eight C-H···Br hydrogen bonds (Fig. 4).

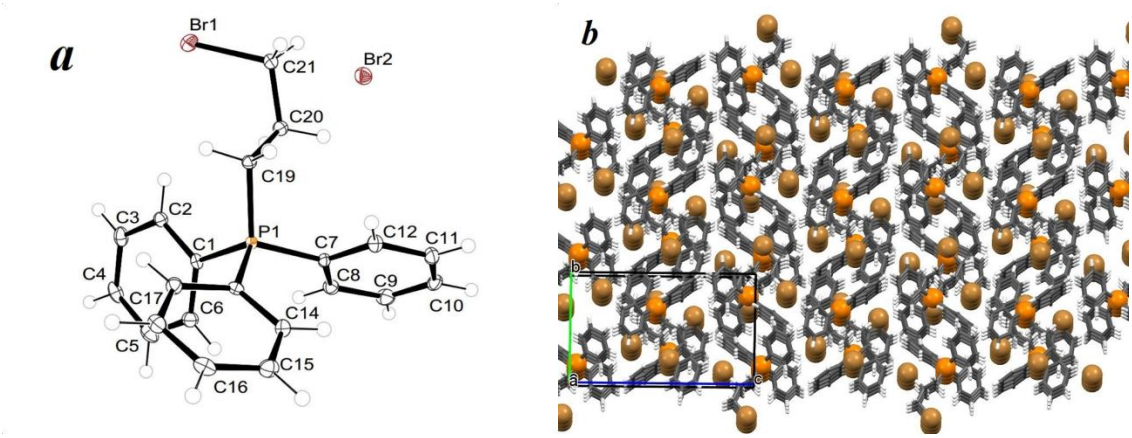


Figs. 3. a) The ORTEP and b) molecular crystal packing diagrams for compound I, with 50% probability displacement ellipsoids.

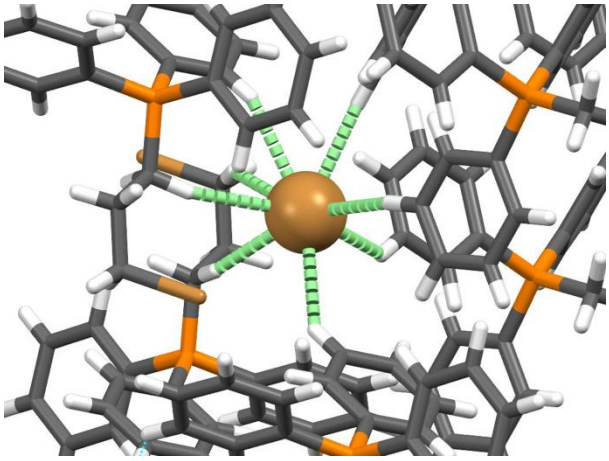

Fig. 4. C-H···Br contacts in I.

The compound II crystallizes in the monoclinic system with $P2_1/c$ space group with Z'=1, Z = 4. The asymmetric unit of this compound contains one propane 3-bromo-1-(triphenyl phosphonium) cation and one tribromide anion. The ORTEP view of compound II is shown in Fig. 5a. Similar to I, the structure of the cationic unit has a slightly distorted tetrahedral geometry at the phosphorous atom. The bond angles around the P atom is in the range of 107.13(15)$^o$ to 111.90(15)$^o$. The crystal packing of II shows a significant number of C-H···Br hydrogen bonds which appear the dominant interaction in the stabilization of supramolecular architecture (Fig. 5b). In addition, there is Br···π interaction between the bromine atom

of the cationic moiety and phenyl ring of adjacent molecule with 3.456(1) Å Br1 to C13-C18 plane centroid and $C_{21}$-$Br_1$···Cg (Ph) angle of 22.433(2)˚ (Fig. 6).

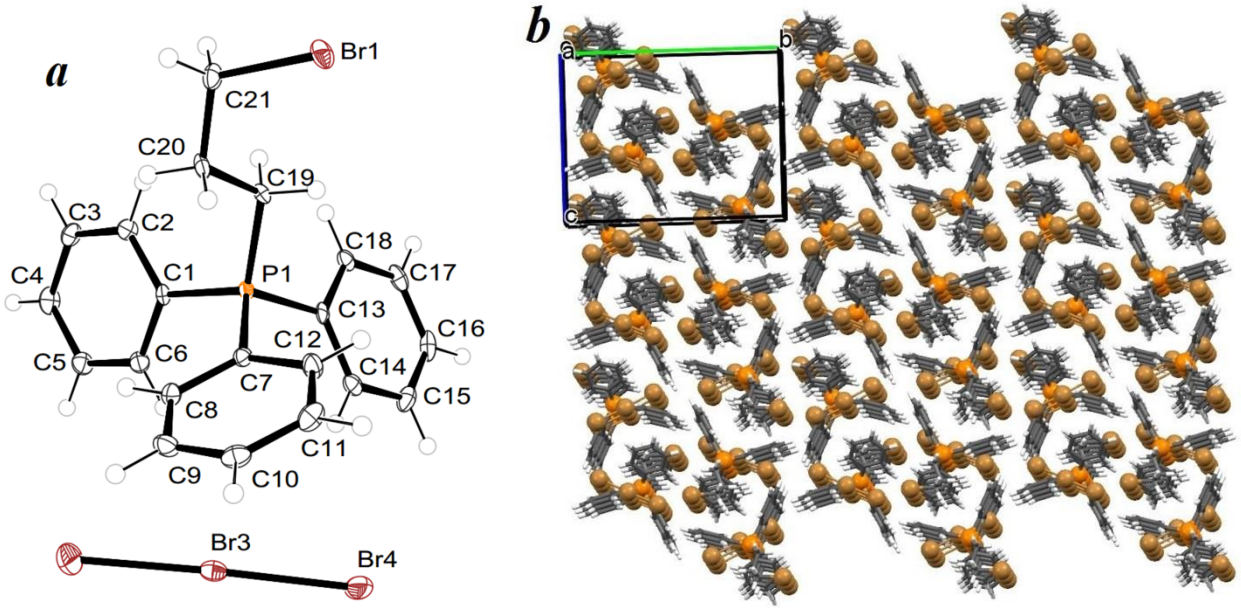


Figs. 5. a) The ORTEP and b) molecular crystal packing diagrams for compound II, with 50% probability displacement ellipsoids.

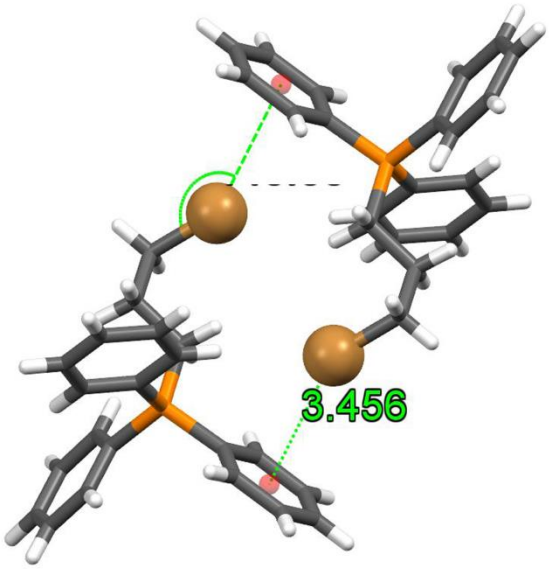


Fig. 6. Br···π interaction between bromine atom of cationic moiety and phenyl ring of the adjacent molecule in compound II.

Comparing the structures of I and II indicates that the different anionic moiety, bromide or tribromide affect the directional interactions between anionic and cationic units as would be expected and therefore

different supramolecular aggregation are observed for these structures. In both structures, however, C-H···π interactions which play an important role in their molecular aggregation are present.

### 2.2. Hirshfeld surface analysis

The Hirshfeld surface of a molecule in a crystal is manufactured by partitioning space in the crystal into areas where the electron distribution of a sum of spherical atoms for the molecule (the *promolecule*) dominates the corresponding sum over the crystal (the *procrystal*). Following Hirshfeld, a molecular weight function $w(r)$ defined:

$$w(r) = \frac{\rho_{promolecule}(r)}{\rho_{procrystal}(r)}$$

$$w(r) = \frac{\sum_{A\epsilon molecule}\rho_A(r)}{\sum_{A\epsilon crystal}\rho_A(r)}$$

$\rho_A(r)$ is a spherically averaged atomic electron density centered on nucleus A, and the promolecule and procrystal are sums over the atoms belonging to the molecule and to the crystal, respectively.

The Hirshfeld surface is then defined in a crystal as that region around a molecule where $w(r) \geq 0.5$. That is, the region where the promolecule contribution to the procrystal electron density exceeds that from all other molecules in the crystal. The surface shape explains the interactions between molecules in the crystal just as atoms in the molecule. Hirshfeld surfaces including almost all of the existing space around molecules

The function $d_{norm}$ is relates the distances of any Hirshfeld surface point to the nearest nucleus interior ($d_i$) or exterior ($d_e$) to the surface taking into account the van der Waals (vdW) radii of the atoms. $d_{norm}$ is a normalized contact distance, which is defined in turns of $d_i$, $d_e$ and the van der Waals radii of the atoms [32].

$$d_{norm} = \frac{d_i - r_i^{\mathrm{vdW}}}{r_i^{\mathrm{vdW}}} + \frac{d_e - r_e^{\mathrm{vdW}}}{r_e^{\mathrm{vdW}}}$$

The negative value of $d_{norm}$ indicates the sum of $d_i$ and $d_e$ is shorter than the sum of the relevant van der Waals radii, which is considered to be a close contact and is visualized as red color on the Hirshfeld Surfaces. The white color denotes intermolecular distances close to van der Waals contact with $d_{norm}$ equal to zero whereas contacts longer than the sum of van der Waals radii with positive $d_{norm}$ values are colored blue. The combination of $d_e$ and $d_i$ in the form of a 2D fingerprint plot provides summary of intermolecular contacts in the crystal.

The 2D-fingerprint plots of the Hirshfeld surface provide a visual summary of the frequency of each combination of $d_e$ and $d_i$ all over the surface of a molecule, therefore they not only indicate which intermolecular interactions are present, but also the relative area of the surface corresponding to each kind of interaction. In this manner, all interaction types (for example, hydrogen bonding, close and distant van der Waals contacts, C–H···π interactions, π–π stacking) are readily identifiable, and it becomes a straightforward method to classify molecular crystals by the nature of interactions, when examining crystal packing diagrams. These plots are unique for a certain crystal structure and polymorph.

The Hirshfeld surfaces and 2D fingerprint plots, calculated using Crystal Explorer 3.1 from the single crystal structures, were used for visualizing, exploring and quantifying intermolecular interactions [29-31] on the surface of molecule in the crystal lattice for both compounds.

Hirshfeld surfaces mapped with $d_i$ ranging from 1.0095 A˚ (red) to 2.5396 A˚ (blue) for I (Fig. 7 aI) and ranging from 1.0569 A˚ (red) to 2.6822 A˚ (blue) for II (Fig. 7 aII) and mapped with $d_{norm}$ ranging from -0.1259 A˚ (red) to 1.1196 A˚ (blue) for compound I (Fig. 7 bI) and ranging from -0.0863 A˚ (red) to 1.1740 A˚ (blue) for II (Fig. 7 bII) are calculated and plotted using Crystal Explorer software. Hirshfeld surface area of compounds I and II mapped with $d_{norm}$ show intense red spots on the surface near the Br ions which are due to $Br_{inside}\cdots H_{outside}$ contacts and intense red spots near the some of hydrogen atoms of aromatic rings

and aliphatic chain near the surface in molecule which are due to $H_{inside}\cdots Br_{outside}$ contacts in the crystal structures (Figs. 7b).

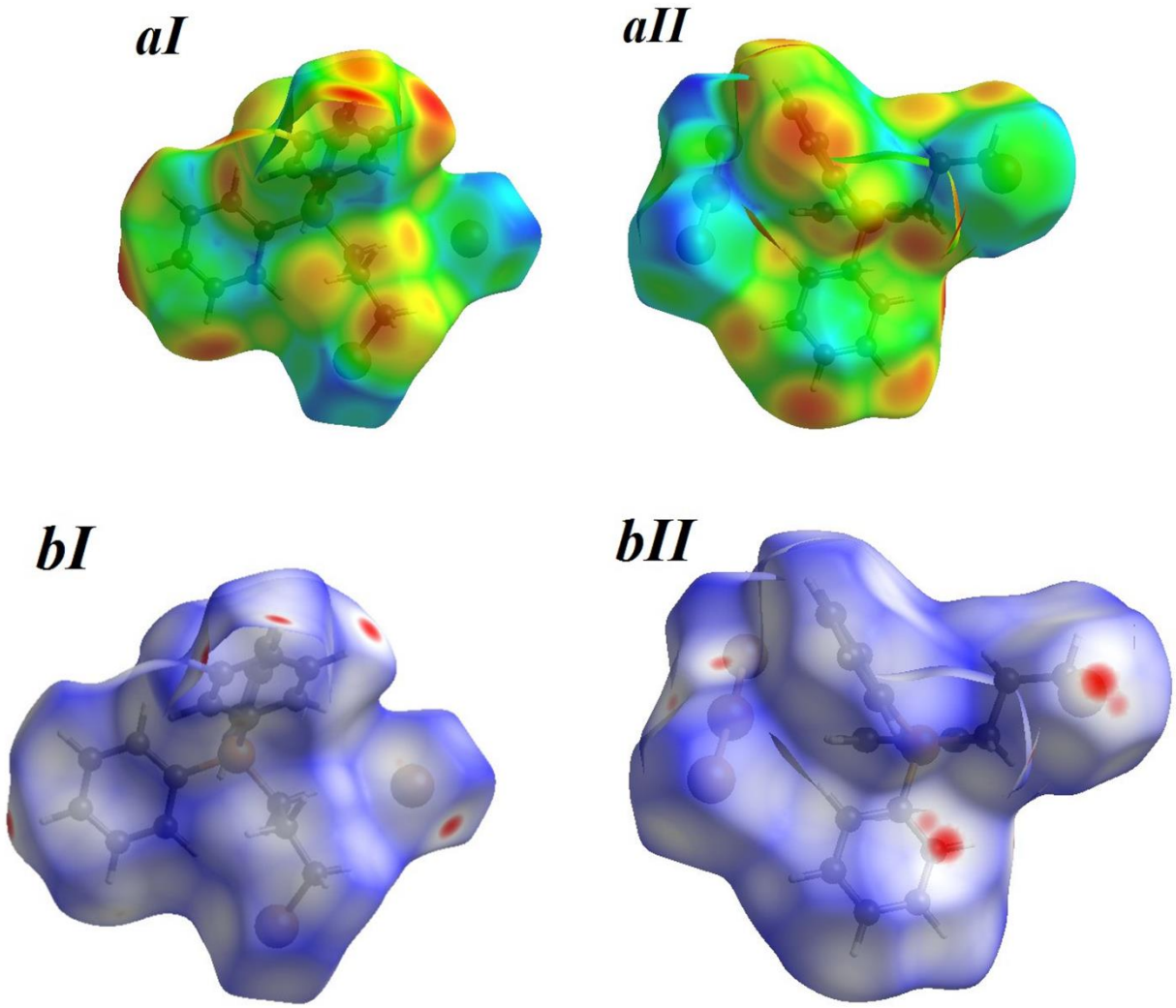


Figs. 7. Hirshfeld surfaces mapped with $d_i$ for compound I (aI) and II (aII) and mapped with $d_{norm}$ for I (bI) and II (bII).

The phosphorus atoms show no contacts in the crystal packing, as would be expected given their tetrahedral coordination. It can therefore be seen that the supramolecular architectures of I and II are mainly controlled by interactions between H and Br atoms. Plots of $d_i$ versus $d_e$ are 2D fingerprint plot which recognizes the existence of different type of intermolecular interactions calculated for I and II (Figs. 8).

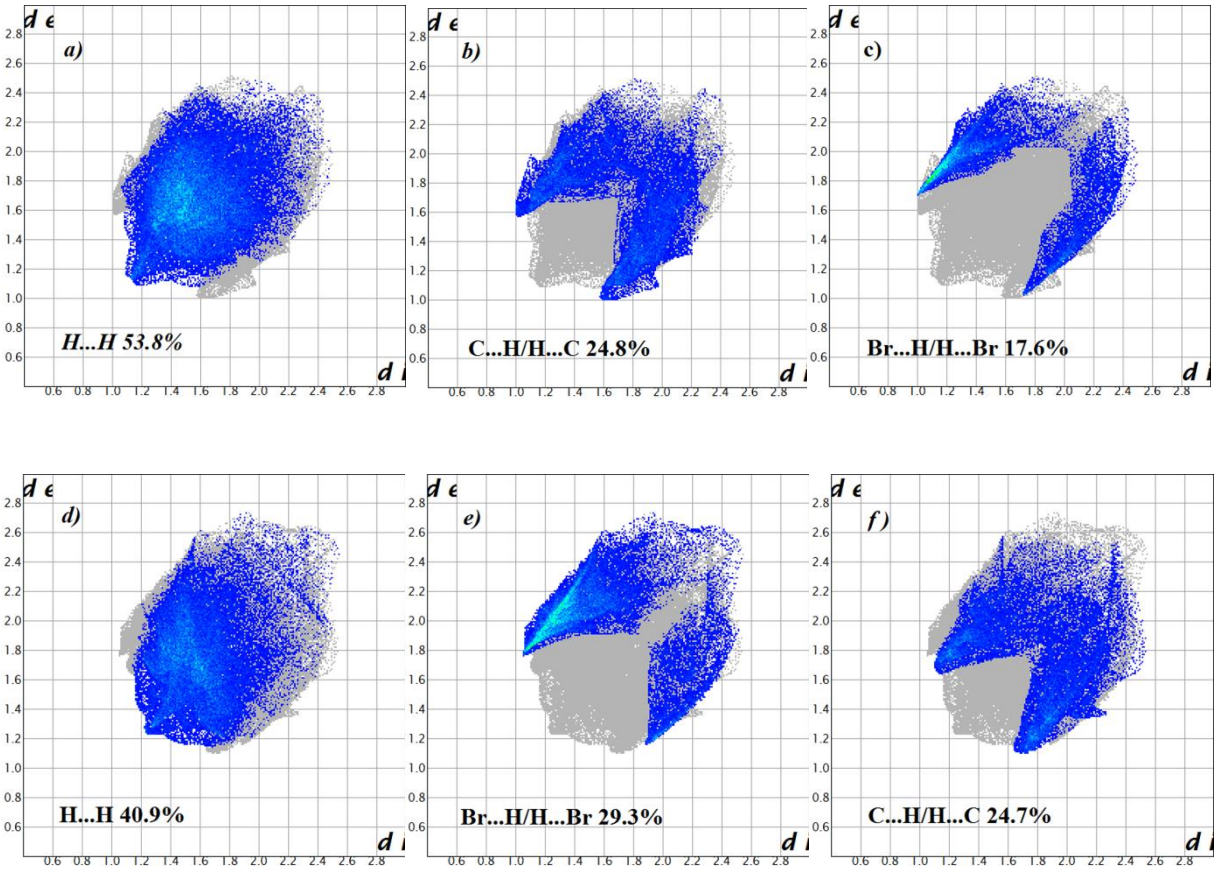


Figs. 8. 2D fingerprint plots for main close contact contributions (in %) in Hirshfeld surface area for a) H···H b) C···H/H···C and c) Br···H/H···Br for compound I cation, d) H···H e) Br···H/H···Br and f) C···H/H···C for compound II cation.

The relative contribution of the different interactions to the Hirshfeld surface indicates that in the cationic unit of compound I, H···H(53.8%), Br···H(17.6%) and C···H(24.8%) contacts account for about 96.2% of the total Hirshfeld surface area and Br···C, Br···Br and C···C have very little effect on the crystal packing. While in the cationic unit of II, the main contacts are Br···H(29.3%), H···H(40.9%) and C···H(24.7%) accounting for about 94.9% of total surface area and other contacts have no major contributions to the total Hirshfeld surfaces in the cation (Figs. 9).

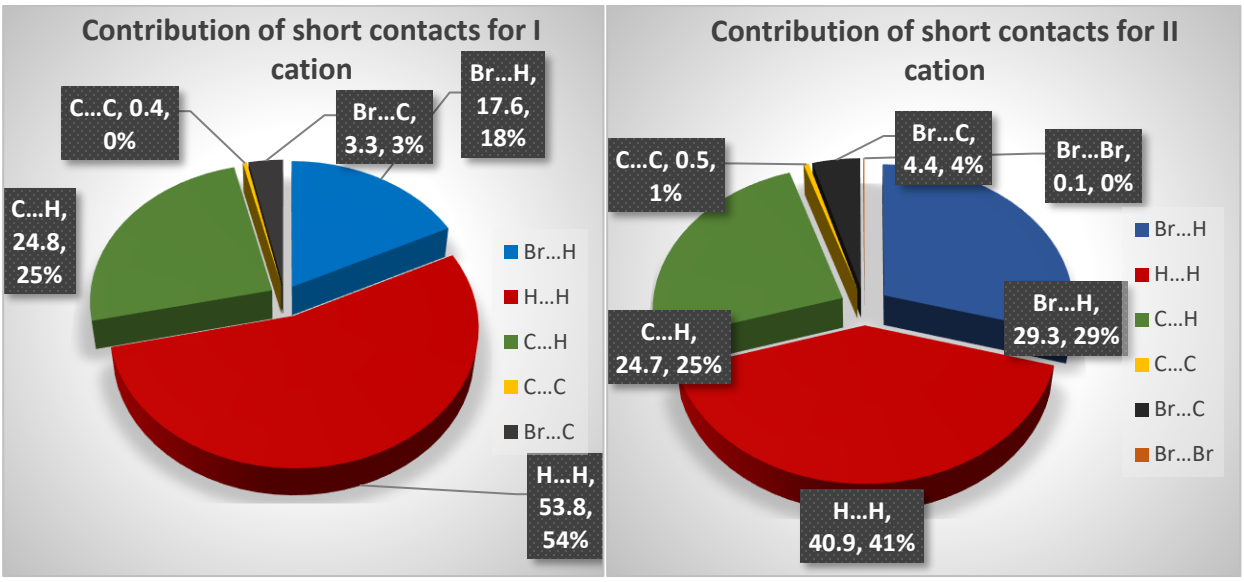


Figs. 9. Percentage contribution of short contacts in compound I and II cations.

The analysis of the 2D fingerprint plot of the cation I shows that Br···H and C···H contacts are illustrated as characteristic wings of the plot, although the most surface area relates to H···H contacts with 53.8% of total surfaces. Moreover, in cation II the Br···H and C···H contacts are illustrated as characteristic wings of the plot, while H···H contacts with 40.9 % of total surfaces.

It is noticeable in 2D fingerprint plots that the most important difference between the intermolecular interactions in I and II is the percentage of Br···H and H···H interactions.

The triphenyl phosphonium cations of I and II are connected by Br···H interactions between nearest neighbors in the unit cell. Nearest intermolecular interactions in I are $Br_2\cdots H_{19B}$ in 2.734 Å, $Br_2\cdots H_{21B}$ in 2.951 Å and $Br_2\cdots H_{12}$ in 3.309 Å (Fig. 10a). Nearest intermolecular interactions in II are $Br_4\cdots H_{14}$ in 2.82 Å, $Br_3\cdots H_6$ in 3.052 Å and $Br_4\cdots H_{15}$ in 3.222 Å (Fig. 10b).

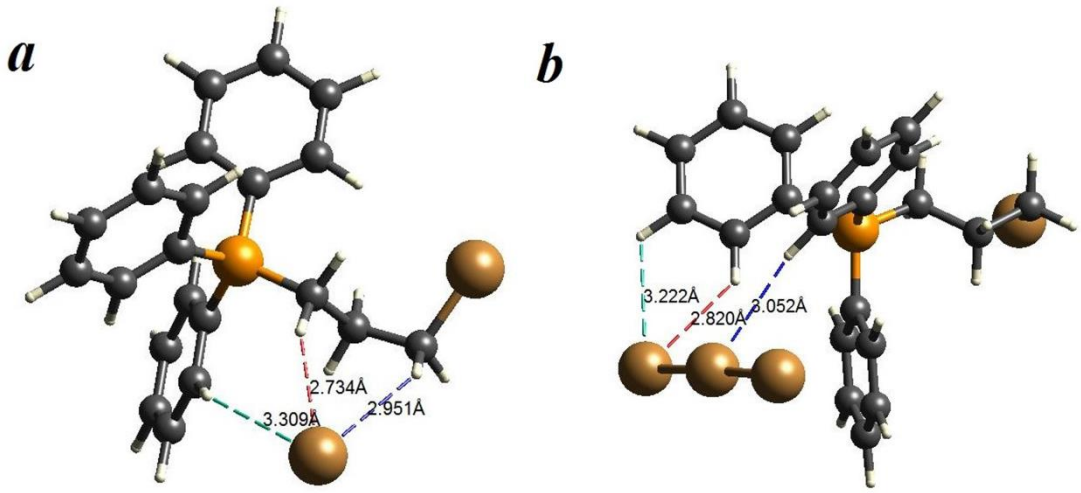


Figs. 10. a) Nearest close contacts in I and b) nearest close contacts in II.

Intra and intermolecular close contacts (up to 3.5 Å) for I and II calculated by Crystal Explorer and Mercury software packages and are tabulated in Table S4 in supporting information.

Moreover, the quantitative measurements of Hirshfeld surfaces for compounds I and II show that the molecular volume, surface area and asphericity of II are bigger than I because of bigger tribromide anion and the globularity of both compounds are nearly same and the comparison of bare cations shows that although the chemical structures and atomic compositions are similar, the tribromide anion enabled an increase in the molecular volume and surface area and decrease in the globularity and asphericity (Table 1). In other words, comparing the tribromide to the bromide anion, the tribromide anion could pull the cation toward itself and cause an increase in the molecular volume and surface area of cation.

Table 1. Quantitative measures of Hirshfeld surfaces for compound I and II and their cations.

| Quantitative measures of Hirshfeld surfaces | molecular volume ($V_H$) Å$^3$ | surface area ($S_H$) Å$^2$ | globularity (G) | asphericity (**Ω**): |
|---|---|---|---|---|
| Compound I | 460.64 | 398.23 | 0.724 | 0.007 |
| Compound II | 542.97 | 442.51 | 0.727 | 0.016 |

| | | | | |
|---|---|---|---|---|
| Compound I cation | 421.75 | 364.06 | 0.747 | 0.013 |
| Compound II cation | 426.94 | 372.24 | 0.737 | 0.005 |

### 2.3.Computation studies

The DFT calculations were performed by using the Gaussian software package, at the B3LYP level with 6-311++G (d, p) basis sets for both compounds I and II. The bond lengths, bond angles and dihedral angles were compared with those obtained from X-ray crystallographic data. The calculation results showed a satisfactory correlation between the theoretical and experimental structural parameters of cations. Significant differences in the optimized DFT and experimental XRD geometries were observed in the location of anions in I and II. In compound I, DFT calculation optimized $Br^-$ anion at the back of molecule and far from Br1 ($d_{Br1-Br2}$ = 9.479 Å) while crystallography data shows that the anion is located at front of molecule near to Br1 ($d_{Br1-Br2}$ = 5.368 Å). While in compound II, although DFT predicted that $Br_3^-$ anion is located at front of molecule near to Br1 ($d_{Br1-Br3}$ = 5.185 Å, Br3 is the atom center of $Br_3^-$ anion), the experimental results show that the anion is located at back of molecule and far from Br1 ($d_{Br1-Br3}$ = 9.366 Å) (Table S6 in supporting information).

Vibrational frequencies of title compounds were calculated by B3LYP/6-311++G (d, p) method. There are 129 vibrational modes for I. The high intensity frequencies of I was calculated at 2979.79 and 3008.95 $cm^{-1}$ which were assigned to for the symmetric stretching of C-H in propane chain and asymmetric stretching of C-H in aromatic rings, Moreover, the vibrational modes at 1468.47, 1284.67, 741.27 and 536.23 $cm^{-1}$ were assigned to symmetric scissoring, symmetric wagging, rotational vibration of C-C bonds and stretching of the P-$C_{arom}$ bond, respectively. For II, 135 vibrational modes were calculated by B3LYP/6-311++G (d, p) method. High intensity frequencies calculated at 2968.31 $cm^{-1}$ for the symmetric stretching of C-H in propane chain, 3197.54 $cm^{-1}$ for symmetric stretching of $C_{arom}$-H, Moreover, vibrational modes at 1117.47,

737.84 and 197.67 $cm^{-1}$ were identified as stretching vibration of P-$C_{arom}$, in plane rocking vibration of C-H and symmetric stretching of Br-Br in tribromide anion respectively.

Natural charge distribution on the whole molecules of I and II were calculated by NBO method calculation indicated that C and Br atoms have a negative character, while P and H atoms have positive ones (Tables S1, S2 in supporting information). HOMO and LUMO are most important orbitals in chemical stability and reactivity of organics. The energy of the HOMO orbitals shows a tendency to donate an electron as a donor in chemical transformations while the energy of LUMO orbitals represent ability to accept an electron as acceptor. HOMO-LUMO energies were calculated by B3LYP/ 6-311++G (d) presented in Figs. 11 and 12 (Table S3 in supporting information).

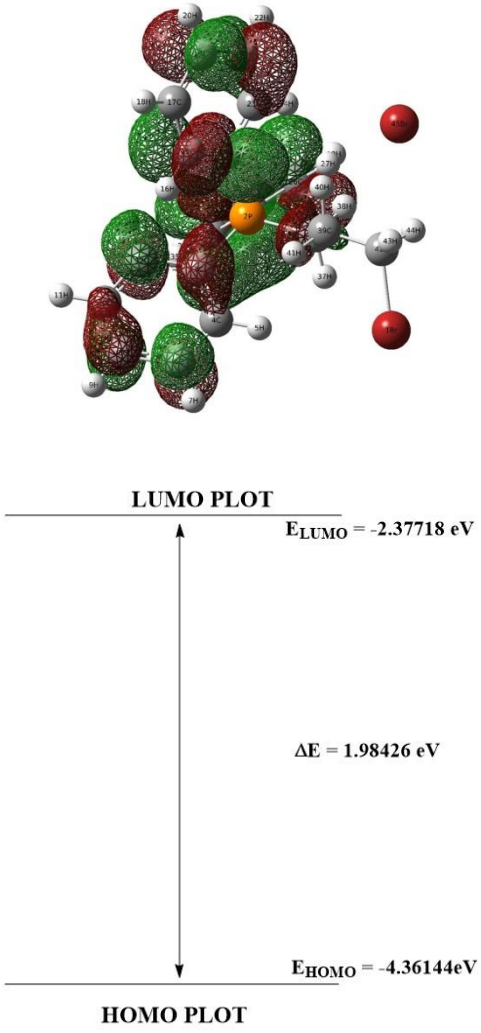

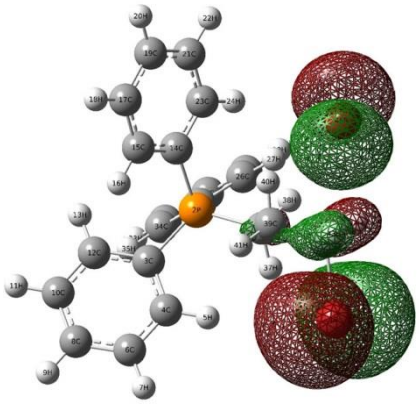

Fig. 11. HOMO-LUMO diagram and energy levels for I.

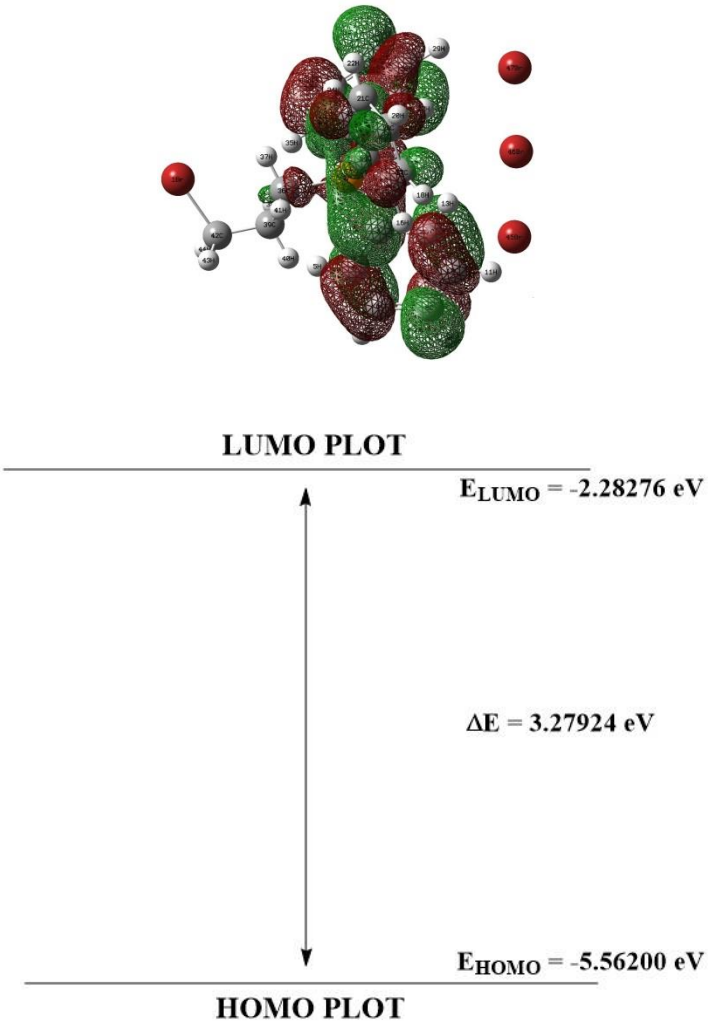

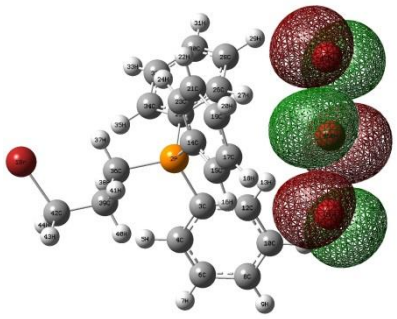

Fig. 12. HOMO-LUMO diagram and energy levels for II.

In addition, binding energies and absorption energies were calculated. The geometry optimizations were performed by B3LYP method which is known to give reliable data on both cations and anions. The standard basis set was 6-31G* which was employed for all of the ions. The energetic results were obtained by single-point calculations at a higher level of theory, being B3LYP/6-311G* based on B3LYP/6-31G* geometries. Binding energies between cation and anion determined as differences between the sum of the energies of each unoptimized bare anion and cation separately (after disconnection) and the energy of optimized ion pair [33, 34]. It is noticeable that anion and cation optimized as an ion pair and that no optimization is needed after disconnection.

Binding Energy of a system consist of ion pairs

$$AC \longrightarrow A^- + C^+$$

$$\Delta E_B = (E_{Anion\text{-}unopt} + E_{Cation\text{-}unopt}) - E_{Ion\ pair\text{-}opt}$$

And absorption energy is defined as differences between the energy of optimized ion pair and sum of energies of each optimized bare anion and cation before pairing:

Absorption Energy of a system consist of ion pairs

$$A^- + C^+ \longrightarrow AC$$

$$\Delta E_{Abs} = E_{Ion\ pair\text{-}opt} - (E_{Anion\text{-}opt} + E_{Cation\text{-}opt})$$

The comparison of the absorption energy and binding energy in compounds I and II shows that $Br^-$ anion can affect only 0.66 Kcal/mol on the deformation of cation whiles the $Br_3^-$ cause deformation of anion about 2.69 Kcal/mol (Table S5 in supporting information).

### 2.4. Structural characterization

#### 2.4.1. Thermal properties of title salts I and II

DSC thermograms were collected under a nitrogen atmosphere; show a sharp endothermic peak appearing at 230-232 $^oC$ due to the melting and a broad peak at 330-380 $^oC$ as the decomposition range of I (Fig. 1). In the case of II, there is a sharp endothermic peak at 149-151 $^oC$ due to the melting and a broad exothermic peak at 310-370 $^oC$ the decomposition range for II (Fig. 2).

The TG/DTG /DTA diagram of I shows an endothermic peak at 230 $^oC$ for melting point in DTA blue curve with the smallest decrease in TG red curve (about 1.4 %) and immediately after that an endothermic shoulder and an exothermic peak with a significant decrease in TG curve for phase transformation in the molecule. Finally, there exist a broad endothermic peak about 330-370 $^oC$ in DTA curve and a sharp decrease in TG curve and very broad peak in DTG brown curve for the decomposition of I and 2.79 % remained ash in 520 $^oC$ (Fig. 13).

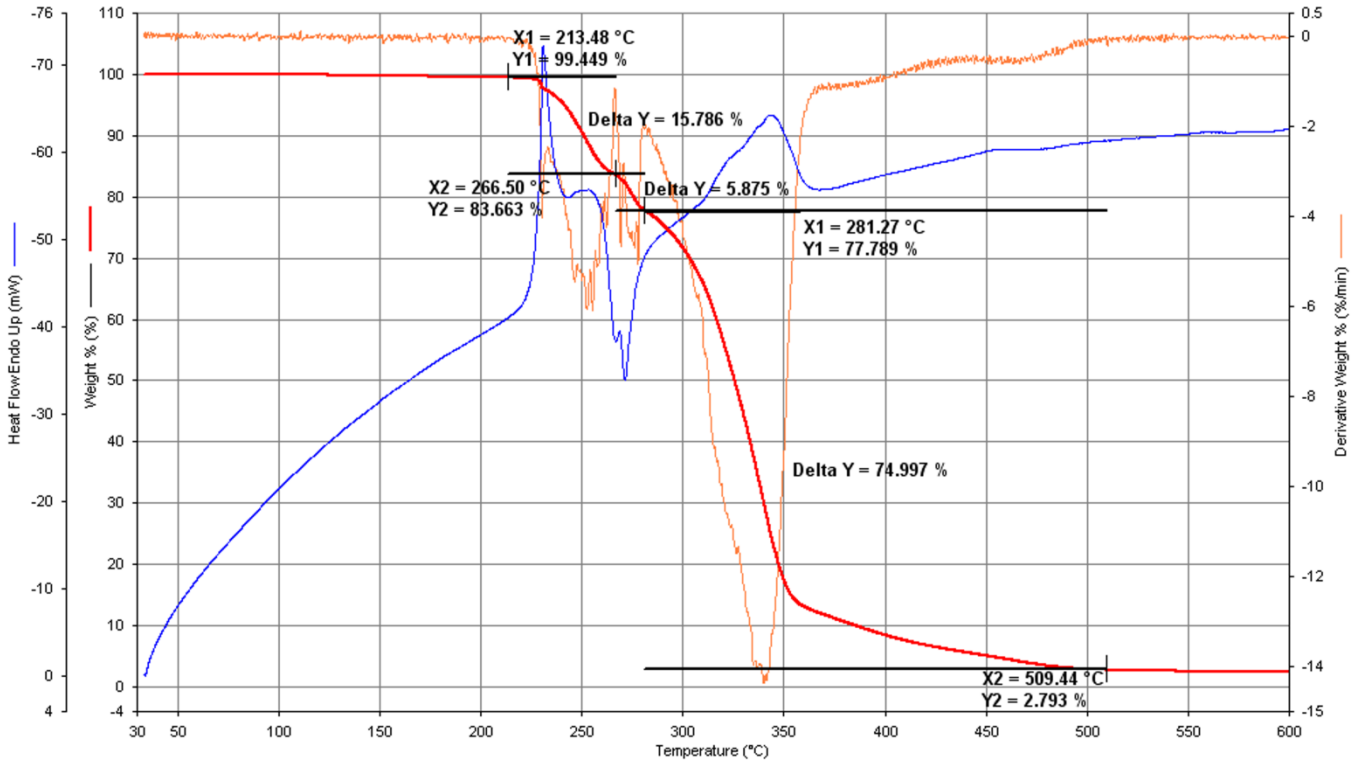


Fig. 13. TG/DTG/DTA thermogram of compound I.

Also for II, the diagram shows an endothermic sharp peak at about 150 $^{o}$C in DTA blue curve and a smallest decrease in TG red curve (0.9 %) for melting point. The broad endothermic peak in the range of 200-250 $^{o}$C in the DTA curve and sharp peaks in DTG brown curve for removal of bromine molecule from tribromide anion were determined about 16 %. An exothermic peak for phase transformation and immediately increase the baseline in the range of 275 -350 $^{o}$C in DTA with a sharp decrease in TG curve was observed. In addition, and broad peak in DTG curve for the decomposition of compound II and about 5 % at 520 $^{o}$C for ash was observable which are completely matched with DSC thermograms (Fig. 14). Both salts have a good thermal stability; they start to decomposing over 300 $^{o}$C. Compound I is slightly more stable than II in comparison and they are very stable on the bench-top in form of crystal or solution in the organic solvent and in contact with air without any change in their color or performance over 3 month.

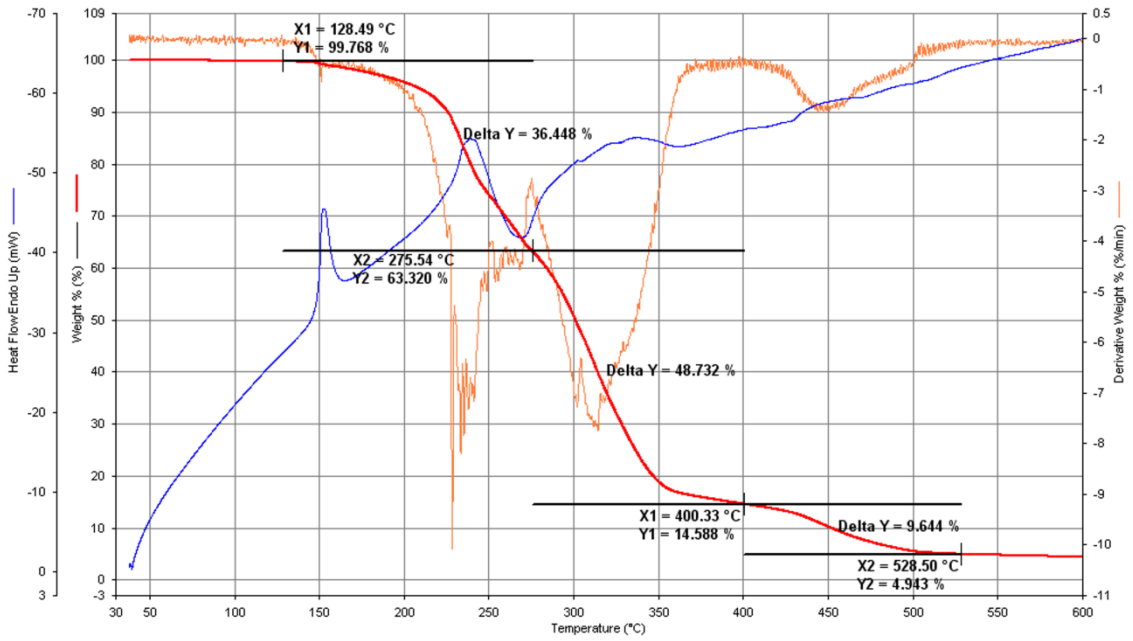


Fig. 14. TG/DTG/DTA thermogram of compound II.

## 3. Experimental section

All reagents including triphenyl phosphine, liquid bromine, 1, 3-dibromopropane, potassium bromide and solvents were purchased from Merck Co. 1, 3-dibromopropane was purified by distillation and tested by GC to give purity more than 99.5%. Solid reagent and salts were recrystallized to give very good purity.

The reaction progresses were monitored by GC. $^{1}H$ NMR, $^{13}C$ NMR, $^{31}P$ NMR spectra were identified by the Bruker AC 500 MHz spectrometer with $D_2O$ and $CDCl_3$ as solvents. DSC thermograms recorded by METTLER - TOLEDO DSC-1 Instrument. TG/DTG/DTA thermograms were recorded by Perkin Elmer Diamond TG/DTA Instrument. Infrared spectra were recorded on a Perkin Elmer –Spectrum 65-FT-IR spectrometer as a KBr disk (4000- 400 $cm^{-1}$ region). GLC analysis was performed with Agilent Technology 6890N Gas Chromatograph with a FID detector and cp-sil 5 CB 30 m, 0.32 mm, 1.2µm capillary column. GC/MS spectra were taken by Varian 3800 GC and Varian Saturn 2000 Ion trap as a detector and cp-sil 8 CB low bleed/ MS 30 m, 0.25 mm, 0.25µm capillary column.

### 3.1. Preparation of Propane 3-bromo-1-(triphenyl phosphonium) bromide ($C_{21}H_{21}PBr_2$), I

To a solution of triphenylphosphine (5.24 g, 20 mmol) in toluene (30 ml) in a 50 ml round –bottom flask equipped with a magnetic stirrer and reflux condenser was added 1,3-dibromopropane (3 ml, 30 mmol, d = 1.989 g/cm$^3$) drop wise by a 2000 µl syringe. Reaction mixture was refluxed for 4 h. After complete reaction, the white precipitate was appeared. The reaction mixture was cooled and the product was filtered and washed with toluene (3 × 10 ml). The white powder was air dried overnight and recrystallized in water as needle shape crystals (5.57 g, 60 % yield). $^1$H-NMR (500 MHz, $D_2O$): (1C, $CH_2$) δ=3.75ppm (m, 2H), (2C, $CH_2$) δ=2.15 ppm (m, 4H) (3C, $CH_2$) δ=3.96 ppm (m, 2H), (aromatic rings hydrogen's) δ=7.64, 7.75(m, 15H). FT-IR: $\bar{\nu}$ = 505,537(s), 685, 723(s), 993(m), 1108(s), 1190, 1328(m), 1432(s), 1482, 1582(m), 2801, 2865(m), 3009(m) cm$^{-1}$. $^{31}$P NMR (200MHz, $CDCl_3$): one strong peak at 35.5 ppm for P atom.

### 3.2. Preparation of Propane 3-bromo-1-(triphenyl phosphonium) tribromide ($C_{21}H_{21}PBr_4$), II

To a solution of KBr (2.38 g, 20 mmol) in $H_2O$ (30 ml) in a 50 ml beaker, liquid bromine was added (1.24 ml, 20 mmol) drop wise with continuous magnetic stirring. The bromine layer disappeared after 30 min. The produced $KBr_3$ solution then added to a solution of propane 3-bromo-1-(triphenyl phosphonium) bromide I (4.176 g, 9 mmol) in water in 2 min. The solution was mixed for over 30 min. The yellow precipitate was filtered and washed with cooled water (3 × 10 ml). The product was air dried overnight and recrystallized in $CHCl_3$ (10.5 g, 94 %), m.p. 150$^o$C (by DSC).

$^1$H-NMR (500 MHz, CDCl3): (1C, $CH_2$) δ=3.58 ppm (m, 2H), (2C, $CH_2$) δ=2.26 (m, 2H), (3C, $CH_2$) δ=3.62 (m, 2H), (aromatic rings hydrogen's) δ=7.76, 7.87(m, 15H). $^{13}$C-NMR (125 MHz, $CDCl_3$): δ=21.8-22.2(m, C20), δ=26.1(m, C21), δ=33.1- 33.3(m, C19), δ=76.7- 77.2 triplet for $CDCl_3$ (solvent), δ=117, 130, 133, and 135 (Benzene rings carbons). $^{31}$P-NMR (200MHz, $CDCl_3$): one strong peak at 35.1 ppm for P atom. $^1$H-NMR spectra of two compounds were taken by 500 MHz spectrometer that show four distinctive peaks for carbons 1, 2, 3 and aromatic rings in ratio 2:2:2:15 respectively. Exchange of anion from bromide to tribromide makes very small shifts in peaks (between 0.2- 0.3 ppm).

### 3.3. General experimental procedure for bromination of alkenes

In a typical reaction, the alkene (3 mmol) was dissolved in dichloromethane (5 ml) and stirred well for 2 min. Propane 3-bromo-1-(triphenyl phosphonium) tribromide II (3 mmol) dissolved in dichloromethane (5 ml) and was added to alkene solution drop wise with constant stirring at room temperature. The progress of the reaction was monitored by TLC and GC. After completion of the reaction and disappearance of the yellow-orange color of reagent II, the solvent evaporated and diethyl ether was added (3×5 ml). The mixture was filtered and the solvent evaporated. The crude product thus obtained and then subjected to a short column of silica gel using a mixture of n-hexane and ethyl acetate (8:2) as the eluent. All of the isolated products are known and physical data have been reported in the literature. The main products, reaction times and isolated yields are tabulated in Table 3. To confirm, the products were subjected to DSC and GC/MS and spectra were compared and validated with the NIST library (see supporting information).

The reusability or recyclability of tribromide salt was tested by regenerating of used brominating salt. The used salt was extracted by water and evaporated under vacuum. The bromide salt, I, was treated with $KBr_3$ and reused 4 times without significant loss of its performance.

Table 3. Bromination of alkenes by compound II in $CH_2Cl_2$ at room temperature

| Entry | Substrate | Product[a] | Reaction time (h) | Isolated Yield[a] ( %) |
|---|---|---|---|---|
| 1 | 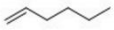 | 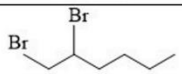 | 0.5 | 92 |
| 2 | 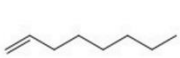 | 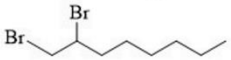 | 0.5 | 95 |
| 3 | 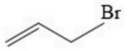 | 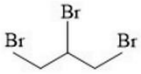 | 0.5 | 97 |
| 4 |  | 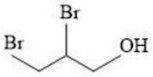 | 0.5 | 88 |
| 5 | 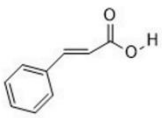 | 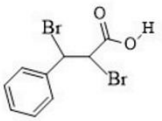 | 2 | 85 |
| 6 | 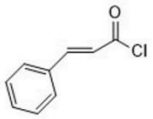 | 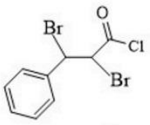 | 4 | 80 |
| 7 | 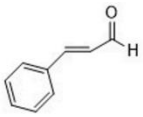 | 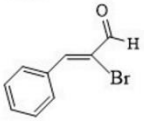 | 4 | 85 |
| 8 |  | 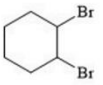 | 0.5 | 95 |
| 9 | 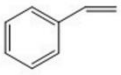 | 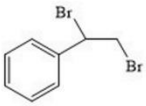 | 0.5 | 95 |
| 10 | 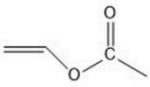 | 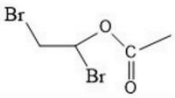 | 0.5 | 90 |

[a]Determined after separation from starting material by DSC, GC and GC/MS

## 4. X-ray crystallography analysis

X-ray diffraction experiments on I and II were carried out at 100(2) K on a Bruker APEX II diffractometer using Mo-$K_\alpha$ radiation ($\lambda$ = 0.71073 Å). Data collections were performed using a CCD area detector from a single crystal mounted on a glass fibre. Intensities were integrated in SAINT [35] and absorption corrections based on equivalent reflections were applied using SADABS [36]. Both of the structures, I and II were solved using ShelXT [37] and refined by full matrix least squares against $F^2$ in ShelXL [38, 39], using Olex2 [40]. All of the non-hydrogen atoms were refined anisotropically. While all of the hydrogen atoms were located geometrically and refined using a riding model. In the case of II the data were found to be twinned and refined against an hklf5 file, with a refined twin scale

fraction of 01247(14). The structural resolution procedure was performed using WinGX crystallographic software package [41]. Crystal structure and refinement data are given in Table 4. CCDC1907510-1907511 contains the supplementary crystallographic data for this paper. These data can be obtained free of charge via www.ccdc.cam.ac.uk/retrieving.html (or from the Cambridge Crystallographic Data Centre 12, Union Road, Cambridge, B2 1EZ; UK, fax +441223336033; or deposit@ccdc.cam.ac.uk).

**Table 4. Crystal data and structure refinement for I and II.**

| Identification code | I | II |
|---|---|---|
| Empirical formula | $C_{21}H_{21}Br_2P$ | $C_{21}H_{21}Br_4P$ |
| Formula weight | 464.17 | 623.99 |
| Temperature/K | 100(2) | 100(2) |
| Crystal system | monoclinic | monoclinic |
| Space group | $P2_1/c$ | $P2_1/c$ |
| $a$/Å | 11.0198(2) | 9.7192(6) |
| $b$/Å | 10.0935(2) | 17.1447(11) |
| $c$/Å | 17.4446(3) | 13.2553(9) |
| α/° | 90 | 90 |
| β/° | 104.7380(10) | 92.770(4) |
| γ/° | 90 | 90 |
| Volume/Å$^3$ | 1876.50(6) | 2206.2(2) |
| Z | 4 | 4 |
| $\rho_{calc}$g/cm$^3$ | 1.643 | 1.879 |
| μ/mm$^{-1}$ | 4.405 | 7.373 |
| F(000) | 928.0 | 1208.0 |
| Crystal size/mm$^3$ | 0.764 × 0.429 × 0.276 | 0.421 × 0.299 × 0.163 |
| Radiation | MoKα (λ = 0.71073) | MoKα (λ = 0.71073) |
| 2θ range for data collection/° | 3.822 to 55.856 | 3.886 to 55.898 |
| Index ranges | $-14 \le h \le 14$,<br>$-13 \le k \le 7$,<br>$-23 \le l \le 22$ | $-12 \le h \le 12$,<br>$-22 \le k \le 22$,<br>$0 \le l \le 17$ |
| Reflections collected | 16880 | 5266 |
| $R_{sigma}$ | $R_{sigma}$ = 0.0210 | $R_{sigma}$ = 0.0452 |
| Data/restraints/parameters | 4491/0/217 | 5266/6/236 |
| Goodness-of-fit on $F^2$ | 1.023 | 1.025 |
| Final R indexes [I>=2σ (I)] | $R_1$ = 0.0200,<br>$wR_2$ = 0.0437 | $R_1$ = 0.0347,<br>$wR_2$ = 0.0671 |
| Final R indexes [all data] | $R_1$ = 0.0246,<br>$wR_2$ = 0.0451 | $R_1$ = 0.0492,<br>$wR_2$ = 0.0711 |
| Largest diff. peak/hole / e Å$^{-3}$ | 0.42/-0.53 | 0.69/-0.95 |

## 5. Conclusion

In this study, the synthesis, characterization and uses of a mild and safe mono cationic phosphonium salt for bromination of the organic substrate are reported. The bromination agent in title salts also has been used as mild brominating and oxidizing agent to selective bromination of C-C double bonds in comparison with very active, non–selective and toxic molecular bromine in very harsh conditions. Reusability or recoverability of tribromide salts is one of the interesting factors that predominate over molecular bromine as these salts can be used and recycled several times without any significant decrease in their performances**.** Ease of getting bromine in aqueous solutions and release of bromine in organic solvents is another important aspect of phosphonium based tribromide reagents.

Also in the present paper, the crystal structure, the DFT calculations, analysis of Hirshfeld surfaces and fingerprint plots, as well as spectroscopic properties and thermal behavior of the title salts are reported.

**Acknowledgments**

The authors are grateful for partial support of this work (grant number 3/45675) by Ferdowsi University of Mashhad Research Council. We would like to especially thank Petrochemical Research and Technology Co to provide DSC thermograms, GC chromatograms and mass spectra.

We hereby acknowledge that part of this computation was performed on the HPC (High Performance Computing) center of Ferdowsi University of Mashhad.

**References**

[1] Xue, Y., Xiao, H. and Zhang, Y., International journal of molecular sciences. 16 **(2015)** 2 3626-3655

[2] Bernard, A., Kumar, A., Jamir, L., Sinha, D. and Sinha, U. B., Acta Chimica Slovenica. 56 **(2009)** 2 457 - 461

[3] Chaudhuri, M. K., Khan, A. T., Patel, B. K., Dey, D., Kharmawophlang, W., Lakshmiprabha, T. and Mandal, G. C., Tetrahedron letters. 39 **(1998)** 44 8163-8166

[4] Kavala, V., Naik, S. and Patel, B. K., The Journal of organic chemistry. 70 **(2005)** 11 4267-4271

[5] Ghandi, K., Green and sustainable chemistry. 4 **(2014)** 01 44-53

[6] Liu, S., Kumatabara, Y. and Shirakawa, S., Green Chemistry. 18 **(2016)** 2 331-341

[7] Werner, T., Advanced synthesis & catalysis. 351 **(2009)** 10 1469-1481

[8] Selva, M., Perosa, A. and Noè, M., Organophosphorus Chemistry169-132 (2016) 45 .

[9] Dey, R. R. and Dhar, S. S., Synthetic Communications. 44 **(2014)** 16 2355-2363

[10] Cristiano, R., Ma, K., Pottanat, G. and Weiss, R. G., The Journal of Organic Chemistry. 74 **(2009)** 23 9027-9033

[11] Cristau, H.-J., Bazbouz, A., Morand, P. and Torreilles, E., Tetrahedron letters. 27 **(1986)** 26 2965-2966

[12] Chiappe, C., Ionic Liquids in Synthesis. 5 **(2008)** 265-568

[13] Ghammamy, S., Mehrani, K., Maleki, S. and Javanshir, Z., Gazi University Journal of Science. 21 **(2008)** 2 33-36

[14] Saikia, I., Borah, A. J. and Phukan, P., Chemical Reviews. 116 **(2016)** 12 6837-7042

[15] Rzelewska, M., Janiszewska, M. and Regel-Rosocka, M., Chemik. 70 **(2016)** 9 515-520

[16] Castillo, J., Coll, M. T., Fortuny, A., Donoso, P. N., Sepúlveda, R. and Sastre ,A. M., Hydrometallurgy. 141 **(2014)** 89-96

[17] Van Esch, G. J., Flame retardants: tris (2-butoxyethyl) phosphate, tris (2-ethylhexyl) phosphate, tetrakis (hydroxymethyl) phosphonium salts.**(2000)** G. World Health Organization

[18] Ovcharov, V., Okhtina, O .and Golovko, D., International Polymer Science and Technology. 29 **(2002)** 10 T/25-T/28

[19] Kanazawa, A., Ikeda, T. and Endo, T., Antimicrobial agents and chemotherapy. 38 **(1994)** 5 945-952

[20] Girard, G., Hilder, M., Zhu, H., Nucciarone, D., Whitbread, K ,.Zavorine, S., Moser, M., Forsyth, M., Macfarlane, D. and Howlett, P., Physical chemistry chemical physics. 17 **(2015)** 14 8706-8713

[21] Hajipour, A. R., Mallakpour, S. E., Imanieh, H. and Pourmousavi, S. A., Journal of Chemical Research. **(2002)** 6 272-275

[22] Kajigaeshi, S. and Kakinami, T., Industrial Chemistry Library. **(1995)** 29-48 Elsevier

[23] Cristiano, R., Walls, A. D. and Weiss, R. G., Journal of Physical Organic Chemistry. 23 **(2010)** 10 904-909

[24] Ma, K. and Li, S., Organic letters. 10 **(2008)** 194158-4155

[25] Jamir, L., Alimenla, B., Kumar, A., Sinha, D. and Sinha, U. B., Synthetic Communications®. 41 **(2010)** 1 147-155

[26] Bora, U., Bose, G., Chaudhuri, M. K., Dhar, S. S., Gopinath, R. and Khan, A. T., Organic Letters. 2 **(2000)** 3 247-249

[27] Salmasi, R., Gholizadeh, M., Salimi, A. and Garrison, J. C., Journal of the Iranian Chemical Society. 13 **(2016)** 11 2019-2028

[28] Bellucci, G., Bianchini, R., Ambrosetti, R. and Ingrosso, G., The Journal of Organic Chemistry. 50 **(1985)** 18 3313-3318

[29] Mckinnon, J. J., Spackman, M. A. and Mitchell, A. S., Acta Crystallographica Section B. 60 **(2004)** 6 627-668

[30] Soman, R., Sujatha, S. and Arunkumar, C., Journal of Fluorine Chemistry. 163 **(2014)** 16-22

[31] Afkhami, F. A., Khandar, A. A., Mahmoudi, G., Maniukiewicz, W., Lipkowski, J., White, J. M., Waterman, R., García-Granda, S., Zangrando, E., Bauzá, A. and Frontera, A., CrystEngComm. 18 **(2016)** 24 4587-4596

[32] Śmiszek-Lindert, W., Michta, A., Tyl, A., Małecki, J., Chełmecka, E. and Maślanka, S., Journal of the Serbian Chemical Society. 80 **(2015)** 12 1489 -1504

[33] Ghashghaee, M., Ghambarian, M. and Azizi, Z., Structural Chemistry. 27 **(2016)** 2 467-475

[34] Ghashghaee, M., Ghambarian, M. and Azizi, Z., Molecular Simulation. **(2018)** 1-10

[35] Bruker, SAINT +v8.38A Integration Engine, Data Reduction Software, Bruker Analytical X-ray Instruments Inc., Madison, WI, USA, **,(2015)**

[36] Bruker, SADABS 2014/5, Bruker AXS area detector scaling and absorption correction, Bruker Analytical X-ray Instruments Inc., Madison, Wisconsin, USA, **,(2014/5**(

[37] Sheldrick, G., Acta Crystallographica Section A. 71 **(2015)** 1 3-8

[38] Sheldrick, G., Acta Crystallographica Section A. 64 **(2008)** 1 112-122

[39] Sheldrick, G., Acta Crystallographica Section C. 71 **(2015)** 1 3-8

[40] Dolomanov, O. V., Bourhis, L. J., Gildea, R. J., Howard, J. A. K. and Puschmann, H., Journal of Applied Crystallography. 42 **(2009)** 2 339-341

[41] Farrugia, L., J. Appl. Crystallogr. 45 **( 2012 )** 849